Title
Targeting RET Kinase in Neuroendocrine Prostate Cancer

Journal
Molecular Cancer Research, 18(8)

ISSN
1541-7786

Authors
VanDeusen, Halena R
Ramroop, Johnny R
Morel, Katherine L
et al.

Publication Date
2020-08-01

DOI
10.1158/1541-7786.mcr-19-1245

Peer reviewed

Targeting RET Kinase in Neuroendocrine Prostate Cancer

Halena VanDeusen[1*], Johnny R. Ramroop[2*], Katherine L. Morel[3], Songyi Bae[1], Anjali V. Sheahan[3], Zoi Sychev[1], Nathan A. Lau[4], Larry C. Cheng[5], Victor M. Tan[5], Zhen Li[6], Ashley Petersen[7], John K. Lee[4], Jung Wook Park[8], Rendong Yang[9], Justin H. Hwang[10, 11], Ilsa Coleman[4], Owen N. Witte[8], Colm Morrissey[12], Eva Corey[12], Peter S. Nelson[4,13], Leigh Ellis[3,11], Justin M. Drake[1,14,15]

Affiliations:

[1]Department of Pharmacology, University of Minnesota-Twin Cities, Minneapolis, MN. [2] Departments of Cancer Biology and Genetics, Comprehensive Cancer Center, The Ohio State University, Columbus, OH. [3]Department of Oncologic Pathology, Dana-Farber Cancer Institute, Boston, MA. [4]Division of Human Biology, Fred Hutchinson Cancer Research Center, Seattle, WA. [5]Graduate Program in Quantitative Biomedicine, School of Graduate Studies, Rutgers University, New Brunswick, NJ. [6]Cancer Metabolism and Growth Program, Rutgers Cancer Institute of New Jersey, New Brunswick, NJ. [7]Division of Biostatistics, School of Public Health, University of Minnesota-Twin Cities, Minneapolis, MN. [8]Department of Microbiology, Immunology, and Molecular Genetics, University of California–Los Angeles, Los Angeles, CA. [9]The Hormel Institute, University of Minnesota, Austin, MN. [10]Department of Medical Oncology, Dana-Farber Cancer Institute, Boston, Massachusetts. [11]Broad Institute of Harvard and MIT, Cambridge, Massachusetts.[12]Department of Urology, University of Washington, Seattle, WA. [13]Department of Medicine, University of Washington, Seattle, WA. [14]Department of Urology, University of Minnesota-Twin Cities, Minneapolis, MN. [15]Masonic Cancer Center, University of Minnesota-Twin Cities, Minneapolis, MN.

Conflict of Interest Statement: Dr. Owen N. Witte currently has consulting, equity, and/or board relationships with Trethera Corporation, Kronos Biosciences, Sofie Biosciences, Breakthrough Properties, Vida Ventures, and Allogene Therapeutics. Dr. Peter S. Nelson has no conflicts relevant to this work, however, he is on advisory boards for Astellas, Jansen, Roche with all compensation less than $10K. None of these companies contributed to or directed any of the research reported in this article. The remaining authors declare no potential conflicts of interest.

Abstract

The increased treatment of metastatic castration resistant prostate cancer (mCRPC) with second-generation anti-androgen therapies (ADT) has coincided with a greater incidence of lethal, aggressive variant prostate cancer (AVPC) tumors that have lost dependence on androgen receptor (AR) signaling. These AR independent tumors may also transdifferentiate to express neuroendocrine lineage markers and are termed neuroendocrine prostate cancer (NEPC). Recent evidence suggests kinase signaling may be an important driver of NEPC. To identify targetable kinases in NEPC, we performed global phosphoproteomics comparing several AR independent to AR dependent prostate cancer cell lines and identified multiple altered signaling pathways, including enrichment of RET kinase activity in the AR independent cell lines. Clinical NEPC patient samples and NEPC patient derived xenografts displayed upregulated RET transcript and RET pathway activity. Genetic knockdown or pharmacological inhibition of RET kinase in multiple mouse and human models of NEPC dramatically reduced tumor growth and decreased cell viability. Our results suggest that targeting RET in NEPC tumors with high RET expression could be an effective treatment option. Currently, there are limited treatment options for patients with aggressive neuroendocrine prostate cancer and none are curative. Implications: Identification of aberrantly expressed RET kinase as a driver of tumor growth in multiple models of NEPC provides a significant rationale for testing the clinical application of RET inhibitors in AVPC patients.

Introduction

Second-generation ADT, such as abiraterone acetate and enzalutamide, have provided life-extending therapies for recurrent or mCRPC patients. However, the utilization of more effective ADT has coincided with an increase in the development of AVPC (1). This subset of mCRPC is characterized by poor prognosis and loss of AR-signaling (2). The absence of AR signaling in AVPC renders the existing hormone targeting treatments ineffective and remaining approved therapies, including platinum-based chemotherapy, offer only limited therapeutic benefits (3). A subset of AVPC tumors are classified as NEPC because they express neuroendocrine genes, which are not typically expressed in prostate adenocarcinoma (AdCa). Recent work has implicated the loss of *RB1* and *TP53* mutations as key alterations in the development of NEPC, and inhibition of kinases such as Aurora A kinase (AURKA), MAPK, or FGFR could provide therapeutic opportunities if selected in the right patient subsets (1,4-6). Even with these new developments, there still remains a critical need to understand the molecular characteristics and kinase signaling pathways of NEPC tumors to identify and validate effective treatment options.

Receptor tyrosine kinases link the extracellular environment to intracellular responses through multiple signaling cascades. These signaling cascades regulate numerous pathways that are frequently altered in transformed cells, including cell growth, metabolism, proliferation, differentiation, invasion, motility, and cell death (7). RET is a receptor tyrosine kinase that is essential for neural crest development and is frequently mutated or translocated in subsets of endocrine tumors such as multiple endocrine neoplasia 2 (MEN2) and papillary thyroid carcinomas, respectively (8). RET can be therapeutically targeted with some success in these tumor types. Recently, RET kinase was identified to be tyrosine phosphorylated in a CRPC patient with small cell neuroendocrine pathology (9) and as an enriched cell surface marker in NEPC (10). Further, RET knockdown reduced tumor growth of an AR-dependent cell line xenograft, LNCaP, *in vivo* (11). However, whether RET inhibition could be exploited as a therapeutic target in the treatment of neuroendocrine prostate cancer is unknown.

Here, we evaluated the phosphoproteome of multiple AR independent and AR dependent prostate cancer cell lines to identify altered kinase signaling pathways that are unique to AR independent prostate cancers. Several downstream signaling networks of RET kinase, and RET kinase itself, were enriched and activated in the AR independent cell lines when compared to AR dependent cell lines. Additionally, RET kinase was overexpressed in NEPC tumors in multiple clinical datasets. We found that the NEPC cell line, NCI-H660, was dependent on RET expression for proliferation and that targeted RET pathway inhibitors, AD80, and two other inhibitors currently being evaluated in the clinic,

LOXO-292 and (12,13), potently induced cell death more effectively than currently approved RET inhibitor therapies, cabozantinib and vandetanib (14,15). Finally, we found that AD80, LOXO-292, and BLU-667, were effective in inducing cell death in NEPC organoid models and AD80 was able to reduce tumor growth of NEPC xenograft tumor models. These results indicate that RET kinase is required for tumor growth of several models of NEPC, and that inhibiting RET induces cell death in neuroendocrine prostate cancer cells that are resistant to current ADT therapies. These results ultimately nominate RET as a key candidate to test further in the development and effective treatment of NEPC.

Material and Methods

Phosphoproteomics of Prostate Cancer Cell Lines

Cultured prostate cancer cells were scraped, pelleted, and snap frozen. Phosphopeptide enrichment and trypsin digestion were performed as previously described (16). Briefly, cells were lysed in 6M guanidium hydrochloride buffer (6M Guanidinium chloride, 100mM Tris pH8.5, 10mM Tris (2-carboxyethyl) phosphine, 40mM 2-chloroacetamide, 2mM Vanadate, 2.5mM Sodium Pyrophosphate, 1mM Beta-glycerophosphate, 10 mg/ml N-octyl-glycoside), sonicated, and cleared. 5mg of total protein was digested with trypsin and a 4G10 antibody-based immunoprecipitation (IP) was used to enrich phosphotyrosine peptides. The IP supernatant containing the phosphoserine/threonine (pS/T) peptides (2.5mg) were de-salted on C18 columns and separated via strong cation exchange chromatography. In separate, parallel reactions the pY and pS/T peptides were enriched from non-phosphorylated peptides using titanium dioxide columns. Finally, the pY and pS/T peptides were each de-salted with C18 tips prior to mass spectrometer analysis (LC-MS/MS with a dual pump nanoRSLC system (Dionex, Sunnyvale CA) interfaced with a Q Exactive HF (ThermoFisher, San Jose, CA) (17)). Technical duplicates were run for all samples and data were analyzed using MaxQuant Andromeda version 1.5.3.30 (parameter settings in (18)) against the Uniprot human reference proteome database with canonical and isoform sequences (downloaded September 2016 from http://uniprot.org). Datasets are accessible through dataset identifiers PXD012970 and PXD012971 (19) through the ProteomeXchange Consortium via the PRIDE partner repository.

Phosphoproteome MS data analysis was performed as previously described (20). For supervised clustering, pY and pS/T data were filtered using a 4-fold change cutoff comparing NEPC vs AdCa from the original excel tables (See Supplemental Tables 2 and 3). We expanded upon our previously published mCRPC dataset (PXD002286) by decreasing the phosphosite localization probability cutoff from 0.99 to 0.75 (16). This increased our identifications nearly 50% and have now reported those extra

identifications in this manuscript as Supplemental Table 6. Hierarchical clustering was performed on mass spectrometry and gene expression data using Cluster (Version 3.0)with the Pearson correlation and pairwise complete linkage analysis (21). Java TreeView version 1.1.6r4 was used to visualize clustering results (22).

Kinase Substrate Enrichment Analysis

KSEA was performed as previously described (23). Briefly, phosphopeptides were rank-ordered by average fold change between AR independent (AVPC) vs AR dependent (AdCa) prostate cancer cell lines. An enrichment score was calculated using the Kolmogorov-Smirnov statistic and statistical significance was calculated via permutation analysis. The normalized enrichment score (NES) was calculated by taking the enrichment score and dividing by the mean of the absolute values of all enrichment scores from the permutation analysis. The Benjamini-Hochberg procedure was utilized to calculate false discovery rate for each kinase. For pY analyses, cutoffs of FDR<0.05, hits>4, and NES>1.3 were used. For pS/T analyses, cutoffs of FDR<0.02, hits>5, and NES>2 were used.

Tissue Culture

Human prostate cancer cell lines LNCaP, VCaP, C4-2, 22Rv1, DU-145, PC3 and NCI-H660 cells were obtained from ATCC. LNCaP, VCaP, C4-2, 22Rv1, DU145, and PC3 cells were grown in appropriate media as recommended by ATCC (Life Technologies) supplemented with 10% fetal bovine serum (Sigma Aldrich) and 1% penicillin-streptomycin (Life Technologies). NCI-H660 cells were grown in Advanced DMEM/F12 (Gibco), with 1X B27 Supplement (Gibco), 10 ng/mL EGF (PeproTech), 10ng/mL bFGF (PeproTech) 1% penicillin-streptomycin, and 1X Glutamax (Life Technologies). LASCPC-01, cMyc/myrAKT, PARCB-1-3 and -5, and EF1 cell lines were obtained from Dr. Owen Witte at UCLA and cultured as described (10,24-26). H660 organoids were cultured as described in (27). Mouse organoids were established by enzymatic digestion of GEMM primary prostate tumor tissue in 5 mg/ml Collagenase type II (Gibco) in adDMEM/F12 (Gibco) media with 10 µM Y-27632 dihydrochloride (Tocris Bioscience). Digested cells were seeded into 100% Matrigel and cultured as described by Drost et. al 2016. NCI-H660 organoids were seeded into Prostate 18 QGel 3D Matrix (QGel) according to manufacturer's instructions and cultured in RPMI-HITES media with B27 supplement (Gibco), 1.25 mM N-acetylcysteine (Sigma), 5 ng/mL EGF (PeproTech), 500 nM A83-01 (Tocris Bioscience), 5 ng/mL FGF2 (PeproTech), 10 ng/mL FGF10 (PeproTech), 10 mM Nicotinamide (Sigma), and 1 µM Prostaglandin E2 (Tocris Bioscience). Culture media was replenished every 4 days and organoids were passaged by sequential digestion in 1 mg/mL Dispase II (Gibco) followed by TrypLE Express (Gibco) and mechanical disruption through a needle to dissociate to single cells before re-suspension as a 3D culture. RET immunofluorescence in SKO and DKO

organoids was followed standard staining procedures using the RET antbody (Cell Signaling Technology E1N8X, 1:100). All cells were grown and maintained in a humidified incubator at 37°C and 5% CO_2.

Dependency Analysis

Gene dependency data is based on pooled genome-scale shRNA screens from DEMETER-adjusted (28) Project Achilles 2.201 data (29). DEMETER scores for RET was ranked for all cell lines was ranked and plotted across 503 cell lines. Of the same data, to statistically compare the patterns of RET dependency in 8 prostate cancer cell lines to other genes, we ranked the DEMETER score of 11280 genes in 8 prostate cell lines and computed the spearman correlation coefficient for each gene dependency relative to RET dependency.

Generating Stable RET knockdown cell lines and cell growth assay

pLKO.1 scramble shRNA and shGFP plasmids were a gift from David Sabatini (Addgene plasmid #1864 and #30323) and two pLKO.1 –shRET plasmids (RET1: CCACCCACATGTCATCAAATT, RET2: GGGCGACCGTACATGACTATA) used to generate the Project Achilles data set were kindly provided by laboratory of Dr. William C. Hahn (Dana-Farber Cancer Institute, Boston, MA) from the RNAi Consortium at the Broad Institute. Lentiviral particles were generated by transfecting 293T cells with 13μg pMDL, 5μg pRev, 7μg pVSVg and 20ug pLKO.1 shRNA plasmid using calcium phosphate. NCI-H660 or PC3 cells were transduced with lentivirus in the presence of polybrene (10 μg/mL). After 72 hours of infection, stable cells were selected by puromycin (0.5 μg/ml for NCI-H660 cells; 1 μg/ml for PC3 cells).

Stable cells were seeded into 96-well plates at cell density of 1000 cells/well (n = 5) for NCI-H660-derived cell lines and 200 cells/well (n = 3) for PC3-derived cell lines. Then, cells were cultured for indicated length of days. Cell culture media of NCI-H660 and PC3-derived stable cell lines was replenished every 5 days or 3 days, respectively. Cell proliferation was measured every 5 days for NCI-H660-derived stable cell lines and every 2-3 days for PC3-derived stable cell lines using WST reagent (Takara).

Immunoprecipitation and Western blots

Cells for western blot analysis were lysed with 1% SDS/2% β-ME and boiled for 10 minutes following a freeze thaw after lysis. The protein concentration was determined using BioRad Quick Start Bradford Protein Assay Kit following manufacturer's protocol. 20μg of protein per lane was loaded into GenScript SurePage 4-12% gel, transferred to a nitrocellulose membrane, blocked in 5% BSA in 1xTBST for one hour at room temperature before incubating in primary antibodies (diluted in 1% BSA in TBST) overnight at 4°C. Membranes were washed with 1xTBST before incubating in Licor IR-conjugated secondary antibodies (diluted 1:5000) for one hour at room temperature, washed again and imaged

using the Licor Odyssey System and adjusted with the Licor Image Studio Lite software (v5.2). The following antibodies were used for western blot analysis at 1:1000 fold dilutions unless otherwise indicated: Total RET (Cell Signaling Technologies E1N8X), phospho ERK1/2 T202/Y204 (Cell Signaling Technologies D13.14.4E), Total ERK1/2 (Cell Signaling Technologies 137F5), pAKT1/2 S473 (Cell Signaling Technologies D9E), AKT (Cell Signaling Technologies C67E7), phosphotyrosine (Millipore Sigma 4G10, 1:500), AR (Santa Cruz sc-7305, 1:500), α-Tubulin (Santa Cruz sc32233), β-Actin (Cell Signaling Technologies 13E5, 1:5000).

For immunoprecipitation analysis, cells were lysed with cell lysis buffer containing 20 mM Tris-HCl (pH 7.5), 150 mM NaCl, 1 mM Na_2EDTA, 1 mM EGTA, 1% Triton, 2.5 mM sodium pyrophosphate, 1 mM beta-glycerophosphate, 1 mM Na_3VO_4, 1 µg/ml leupeptin and 1 mM PMSF. The protein concentration was determined by bicinchoninic acid protein assay (Pierce) according to the manufacturer's instruction. The immunoprecipitation was performed using Dynabeads® Protein A (Life Technologies) following the manufacturer's protocol with modification. Briefly, total RET (Cell Signaling Technologies C31B4, 1:50) antibody was pre-incubated with the beads overnight at 4°C. Then, equal amount of each cell lysate was incubated with the RET antibody-conjugated beads overnight at 4°C. After washing the bead-RET antibody-antigen complex four times with cell lysis buffer, the antigen was eluted with 2x Laemmli Sample Buffer (Bio-Rad)/5% β-ME by heating at 95°C for 5 minutes before analysis by western blot.

LD_{50} value measurement

AD80, BLU-667, cabozantinib, and vandetanib were all obtained from Selleckchem LOXO-292 was obtained from MedChemExpress and all drugs were resuspended in DMSO. Cells were treated with drug for 72 hours prior to the WST assay and viability was measured using the WST reagent (Takara) following manufacturer's protocol. Each concentration data point was conducted in triplicate. Each compound was tested at a minimum of ten dose levels, separated by four-fold dilution concentration intervals, LD_{50} values were calculated using GraphPad Prism 7. Reported values were calculated from a single WST assay, but were confirmed by repeating the entire assay in duplicate.

Organoid dose response

For assays, organoids were seeded as single cells in 40 µL of 33% Matrigel (mouse organoids) or Prostate 18 QGel 3D Matrix (NCI-H660 organoids) in 96-well tissue culture plates and cultured for 2 days at 37°C to allow organoid formation. Once formed, organoids were treated with AD80 (at concentrations of ranging from 0.1 µM to 30 µM), LOXO-292 or BLU-667 (at concentrations ranging from 0.01µM to 100µM), or 10 µM Enzalutamide (MedchemExpress) for 72 hours. After treatment, cells were

stained with 10µL ReadyProbes Cell Viability Imaging Kit Blue/Red (Invitrogen) per well for 30 minutes at room temperature and z-stack images of stained cells were taken using an EVOS FL Auto 2 Cell Imaging System (Invitrogen). The percentage of cell death was calculated by identifying the percentage of PI-positive cells per organoid in at least 10 organoids for each treatment condition and the LD_{50} was calculated in GraphPad Prism 7.

In vivo studies

Experiments were carried out on 8-week-old male NOD-SCID mice in accordance with IACUC approved protocols. Xenografts were generated via subcutaneous injection of $1x10^6$ NCI-H660 cells per animal mixed at a 1:1 ratio with Corning Matrigel Matrix into the right flank. Tumors were allowed to grow to approximately 100-200mm^3 before mice were randomly allocated into vehicle (5% DMSO) or AD80 (10 mg/kg/day in the first experiment or 20mg/kg/day in the second experiment) treatment groups. Dosing proceeded once daily, 5 days a week for 22 days by oral gavage. Tumor volume and animal weight were measured every two days. Tumors volume was measured by caliper and expressed in mm^3 (Tumor Volume = $0.5\ a \times b^2$, where a and b represents long and short diameter respectively).

Immunohistochemistry

Xenograft tumors were formalin fixed paraffin embedded and sectioned following standard procedure. To stain, sections were deparaffinized by baking at 65°C for one hour and hydrated with sequential washes in xylenes, 100% ethanol, 95% ethanol, 70% ethanol and 1xPBS, prior to citrate buffer pH 6.0 antigen retrieval. To stain, tissues were washed with 0.1%TBST, blocked with 2.5% normal horse serum for one hour at room temperature before incubating in primary antibody (RET: Cell Signaling Technologies E1N8X, 1:500 and Ki67: Cell Signaling Technologies 8D5, 1:400) overnight at 4°C in a humidified slide box. Slides were washed with 0.1%TBST and incubated in HRP-conjugated secondary antibody (Vector Laboratories, MP-7500-15) for one hour at room temperature and developed using a DAB peroxidase substrate kit (Vector Laboratories, NC9567138). Reaction was stopped with water before proceeding to counterstaining with hematoxylin for one minute. Slides were de-stained in tap water, dehydrated with ethanol and xylenes and mounted. Tumor sections were imaged on a Zeiss Axiovert A2. Average RET or KI67 staining was determined by color deconvolution followed by measurement of the mean gray value in the DAB channel in Fiji (30). Mean gray value was converted to optical density with the following equation: OD=Log(Max gray value/Mean gray value). Values for images from five distinct fields of view were averaged to create a single data point for each tumor in each treatment group.

Terminal deoxynucleotidyl transferase dUTP nick end labeling (TUNEL) assay

The Click-iT™ Plus TUNEL Assay for In Situ Apoptosis Detection, Alexa Fluor™ 488 Kit was used according to the manufacturer's protocol (Invitrogen). Nuclei were counterstained with Hoechst 33342 (ThermoFisher). A DNase treated positive control section was incubated in 1 U of DNase I diluted into 1X DNase I Reaction Buffer (20 mM Tris-HCl, pH 8.4, 2 mM $MgCl_2$, 50 mM KCl) for 30 minutes at room temperature (Invitrogen). The TUNEL-positive cells in tissue sample slides were identified by comparing to the DNase treated positive control and the no-TdT enzyme negative control. Percent TUNEL positive area was determined by using Fiji to measure the TUNEL positive area divided by total tumor area x100 for each tumor. Adjacent tissue sections were stained with hematoxylin and eosin by the University of Minnesota Clinical and Translational Science Institute Histology & Research Laboratory.

Statistical Analysis

For xenograft tumor volume experiments, means and confidence intervals (CIs) were calculated on the log scale due to skew and reported in terms of geometric means after exponentiation. Tumor growth rates were fit with a linear mixed effect model in R. All other statistical analyses and Pearson correlations were performed using GraphPad Prism 7 with the tests indicated in the figure legends. $P<0.05$ was considered to indicate a statistically significant difference. P values were determined with significance indicated as follows; *p<0.05, **p<0.01, ***p<0.001 and ****p<0.0001.

Results

AR independent cell lines have altered phosphotyrosine and phosphoserine/threonine kinase signaling pathways. To identify the unique kinase signaling pathways required for growth and proliferation of AR independent prostate cancer, we performed phosphoproteomic profiling. We compared AR dependent cell lines (LNCaP, VCaP, C4-2, and 22Rv1), to AR independent cell lines that are resistant to ADT and harbor mutations commonly found in NEPC tumor samples (DU145, PC3, NCI-H660, cMyc/myrAKT, LASCPC-01 (25), EF-1 (10), and PARCB-1,-2,-3, and -5 (26), Supplemental Table 1). Supervised hierarchical clustering between the AR dependent and AR independent groups revealed distinct patterns in phosphoserine/threonine (pS/T) and phosphotyrosine (pY) peptides (Figure 1A and 1B, respectively and Supplemental Tables 2 and 3). Kinase substrate enrichment analysis (KSEA) identified AURKA as the most highly enriched pS/T kinase (Figure 1C) and this kinase has been previously reported to be significantly upregulated in NEPC (4). Interestingly, among the tyrosine kinases, RET kinase was also significantly enriched (Figure 1D), suggesting that RET kinase is activated in AR independent cell lines (full pS/T and pY KSEA results are in Supplemental Tables 4 and 5, respectively). We confirmed that the RET protein is highly upregulated in the NEPC subset of AR independent cell lines

(Supplemental Figure 1). Further investigation into the RET pathway via our cell line-derived and previously published mCRPC rapid autopsy phosphoproteomic datasets (9) (expanded phosphoproteome data set in Supplemental Table 6, see methods) identified hyper-phosphorylation and, in some cases, activation, of several RET pathway targets including MAPK, AKT, and STAT3 (Figure 1E, 1F), further confirming RET pathway activity in AVPC cell lines and tumors.

RET kinase gene expression is upregulated in patients with neuroendocrine prostate cancer. We took advantage of several clinical prostate cancer gene expression datasets to determine whether RET kinase was overexpressed along with known markers of NEPC. Analysis of the University of Washington rapid autopsy dataset (31) which contains multiple metastatic tumors from CRPC patients revealed that the NEPC (AR-negative, NE-positive) subset had enrichment of RET kinase expression concomitant with increased neuronal lineage genes ASCL1 and chromogranin A (CHGA) and decreased luminal epithelial lineage genes AR, NKX3-1, and KLK3 expression (Figure 2A). Among all patient samples included in the dataset, there was a strong correlation between levels of RET and neuronal lineage markers, while there was a negative correlation with RET expression and the AR-responsive genes (Figure 2B). Overall, the NE-positive patient population had increased RET expression compared to the AR positive population (Figure 2C). An additional patient derived xenograft (PDX) transcript dataset comparing metastatic NEPC to metastatic AdCa showed a similar correlation and upregulation of expression of RET and neuronal lineage markers in the NEPC population (Figure 2D, E, and F) (32). This trend was also observed in additional prostate cancer datasets (6,33-35). Overall, these independent datasets demonstrate that RET kinase is frequently overexpressed in clinical NEPC tumors and supports our cell line phosphoproteomic and KSEA analyses, suggesting enhanced RET activity drives NEPC proliferation and survival and therefore nominates RET as a candidate therapeutic target for NEPC tumors.

RET expression correlates with neuroendocrine transcription factors in prostate cancer cell lines and is necessary for NEPC proliferation. The robust levels of RET gene expression in NEPC patient samples suggests it is a potential target in NEPC. To validate the correlation of RET gene expression in prostate cancer cell lines, we examined relative RET dependency in the publicly available pooled genome-scale RNAi screen of 503 cancer cell lines, which includes seven prostate cancer cell lines and one basal prostate cell line (29). We compared the patterns of RET dependency relative to 11,280 genes in the eight prostate cell lines (Supplemental Table 7). As shown in Figure 3A, strong correlations were observed between the dependencies of RET and NEPC driver genes (POU3F2, SOX2, ONECUT2 and ASCL1). In contrast, a negative correlation was seen between the dependencies of RET and AR. AR expectedly showed strong correlation with AR regulators (CTNNB1, NCOA1 and CREBBP). To determine

if RET expression was required for cellular proliferation or viability, we compared the Project Achilles DEMETER scores of RET, highlighting the prostate cancer cell lines (Figure 3B) (28). The DEMETER score indicates how gene suppression affects cell viability compared to all other cell lines upon suppression of the same target gene. Among the seven prostate cancer cell lines, two of the AR independent AVPC cells, PC3 and NCI-H660, exhibited greater relative dependency on RET compared the 501 other cell lines (ranked 10^{th} and 76^{th}, Supplemental Table 8). This indicates RET kinase is required for the growth some AR independent prostate cancer cell lines and not in the AR dependent lines.

We validated the findings from the high-throughput short hairpin RNA (shRNA) screening by generating stable RET knockdown cell lines. The two most RET dependent cell lines from the large-scale screen, PC3 and NCI-H660, were stably transduced with two unique anti-RET shRNA constructs and the downregulation of RET protein or mRNA expression were confirmed (Figure 3C and Supplemental Figure 3A). RET knockdown strongly suppressed the growth of NCI-H660 cells, and to a lesser extent the PC3 cells. Interestingly, this correlates with the relative level of RET protein expression by western blot, which is readily detectible in NCI-H660 cells and much lower in the PC3 cells (Supplemental Figure 1). After 25 days of incubation, the total number of NCI-H660 cells decreased by 81% (shRET1, $p = 0.00013$) and 93% (shRET2, $p = 8.82 \times 10^{-5}$) compared to the scrambled shRNA (shScr) cells (Figure 3D). The number of stable RET knockdown PC3 cells was 45% (shRET1, $p = 0.0021$) and 50% (shRET2, $p = 0.0021$) lower compared to shScr cells at Day 8 (Supplemental Figure 3B). Taken together, this suggests that RET kinase plays a role in enhancing NEPC cell growth and can be an effective therapeutic target for NEPC treatment.

RET kinase inhibitors block RET signaling in NEPC cells. AD80 is a novel, more selective inhibitor of the RET pathway than previous multi-tyrosine kinase inhibitors such as cabozantinib or vandetanib (14,15). However, AD80 still targets multiple other cellular kinases such as p70S6K, SRC, and VEGF receptors (15). We also utilized the newer RET inhibitors, LOXO-292 and BLU-667, which are currently undergoing clinical trials in RET fusion driven solid tumors and are considered specific RET inhibitors with few adverse effects (12,13). To determine if prostate cancer cells are sensitive to RET inhibition, we determined the IC_{50} of AD80, LOXO-292, BLU-667 in our panel of prostate cancer cell lines (Supplemental Figure 4A). AD80 was consistently among the most effective at reducing viability, and the NCI-H660 cells were the most sensitive to AD80 of the RET inhibitors tested (Supplemental Figures 4A-C). To confirm that RET kinase is active and can be inhibited by these drugs, we treated NCI-H660 cells with AD80, LOXO-292, BLU-667, or DMSO for 4 hours and evaluated the tyrosine phosphorylation of RET (36). RET kinase immunoprecipitated from RET inhibitor treated NCI-H660 cells showed a reduction in

total tyrosine phosphorylation, indicating that AD80, LOXO-292, and BLU-667 all inhibit the activation of RET in NCI-H660 cells (Figure 4A). Next we measured the downstream targets of RET by looking at phosphorylation of ERK1/2 and AKT1/2. Interestingly, all three drugs reduced ERK1/2 phosphorylation of residues Tyr202/Try204 in a dose dependent manner, but AD80 was the most effective in reducing phosphorylation of both ERK1/2 and AKT1/2, while having no effect on the total protein levels (Figure 4B). Cabozantinib and vandetanib also decreased the levels of phospho ERK1/2 and AKT1/2 in NCI-H660 cells (Supplemental Figure 4D). Finally, we treated the RET knockdown cells with AD80, LOXO-292, or BLU-667 (Figure 4C). We found that RET knockdown reduced the levels of ERK1/2 phosphorylation and to a lesser extent AKT1/2 (Figures 4D and 4E). The effect of AD80, LOXO-292, and BLU-667 was reduced in the RET knockdown cells, suggesting that RET is required for full activation of ERK1/2 and AKT1/2 (Figure 4D and 4E). The ability of these RET inhibitors to reduce viability (IC50) combined with genetic knockdown of RET in NCI-H660 cells (Figure 3) suggests that RET kinase is critical to the growth and survival of NEPC cells with high RET expression and can be pharmacologically inhibited.

RET inhibition induces cell death in NEPC 3D culture models. We cultured NCI-H660 cells as 3D spheroids and tested the ability of AD80 to induce cell death (Supplemental Figure 4E). The calculated LD_{50} for the NCI-H660 organoids was 1.4μM, slightly higher than cells in 2D culture. The organoids clearly displayed an increase in dead cells at higher doses of AD80 (Supplemental Figure 4F). We extended our RET inhibitor treatment studies to a second organoid model of NEPC (5). Tumors derived from the prostate epithelium of *Pten*$^{-/-}$*Rb*$^{-/-}$ (DKO) mice express higher levels of RET mRNA than *Pten*$^{-/-}$ (SKO) or wild type (WT) animals (Supplemental Figure 5A) (5). Immunofluorescence staining also confirmed an increase of RET kinase protein in the DKO organoids and low to absent RET kinase in the SKO organoids (Supplemental Figure 5B). The DKO organoids were also resistant to enzalutamide treatment, mimicking the ADT resistant characteristic of NEPC prostate cancer cells that express high levels of RET (Supplemental Figure 5C). Treating the DKO organoids with increasing concentrations of AD80, LOXO-292, or BLU-667 induced a dose-dependent increase in cell death, as assayed by live-dead PI staining of the organoids (Figures 5A-D). All three drugs displayed a similar LD50, suggesting that RET inhibition is effective in preventing tumor growth in a second model of NEPC.

AD80 reduces growth of NEPC xenograft tumors *in vivo* by increasing cell death. To test the efficacy of AD80 in an *in vivo* model system of NEPC, we generated NCI-H660 xenograft tumors in NOD-SCID mice. Once tumors reached 100-200 mm^3, mice were randomized and placed into one of two treatment groups: Control (DMSO) or 10 mg/kg AD80 (Figure 6A). Over the course of the 22-day treatment, AD80 treated tumors showed a significant reduction in overall tumor volume (Figure 6B) without a significant

effect on animal weight (Figure 6C). This experiment was repeated in a second cohort of mice with 24 days of treatment and higher dose of AD80 (20 mg/kg) (Supplemental Figure 6). The higher dose of AD80 was associated with increased toxicity but showed similar inhibition of tumor growth throughout the 24-day treatment (Supplemental Figure 6A, B, C). To interrogate the molecular characteristics of AD80 treatment, the tumors (Figure 6D) were fixed and sectioned for staining. Sections stained with hematoxylin & eosin (H&E) showed similar tumor morphology (Figure 6E and Supplemental Figure 6D). IHC staining for RET showed similar expression and localization among the treatment groups (Figures 6E, 6F and Supplemental Figures 6D, 6E). There was also no difference in tumor proliferation as assayed by Ki67 staining among the treatment groups in either cohort of mice (Figures 6E, 6G, Supplemental Figures 6D and 6F). However, TUNEL staining showed large regions of positive staining and the percentage of total tumor area that stained positive trended higher in the AD80 treated groups (Figures 6E and 6H and Supplemental Figures 6D and 6G). Taken together, these results suggest that AD80 treatment is effective in limiting tumor growth by inducing cell death in neuroendocrine cells with high RET expression and that the specific population of patients that have high RET expression, are refractory to ADT, and have few remaining therapeutic options may benefit from RET kinase inhibitor therapies.

Discussion

Increasing evidence points to the activation of kinase pathways as possible key mechanisms that bypass AR-targeted therapies and allow the tumors to continue to survive such a harsh therapeutic environment (1,4,20,23). Utilizing phosphoproteomics, we showed that AR independent cell lines have altered kinase signaling pathways compared to AR-driven adenocarcinomas, which includes activation of RET kinase. Multiple proteins downstream of the RET kinase pathway were phosphorylated on activating residues in both the cell line and in mCRPC autopsy patient samples. RET mutations or activating rearrangements are drivers of tumor development and growth in MEN2, medullary thyroid cancer and small cell and non-small cell lung cancers, and drugs targeting RET can extend survival of these patients (37-39). Cabozantinib, which inhibits RET kinase and other receptor tyrosine kinases including VEGR1/2, has extended survival in certain cancers with activating RET mutations (40,41). In prostate cancer, cabozantinib showed promise in phase II clinical trials but failed to meet the endpoint criteria in phase III trials (NCT01605227) (42,43). However, this was tested in a non-stratified patient population and did not focus on NEPC or patients with high RET expression (44). A retrospective evaluation of post-docetaxel patients with CRPC in the COMET-1 and COMET-2 phase III clinical trials where cabozantinib was compared with prednisone and prednisone plus mitoxantrone suggest a sub population exists that

may benefit from cabozantinib treatment, highlighting the importance of molecular stratification of patients for individualized treatments (42,43,45). Recently, RET knockdown in a prostate AdCa cell line, LNCaP, was reported to restrict tumor growth, but it remains unclear if and how RET contributes to tumor progression in NEPC (11).

We found that overall RET expression in prostate cancer patient samples is highly variable, but that RET kinase expression correlated very strongly with NEPC. In the datasets we analyzed, there were examples of metastatic and treatment induced NEPC tumors (based on molecular and pathological features) that lacked RET gene expression. Inversely, there were also patients classified as AR-positive adenocarcinomas that displayed high levels of RET gene expression but lacked expression of other neuroendocrine lineage markers (Figure 2 and Supplemental Figure 2). It is important to note that the transition from AdCa to NEPC may be dynamic (5) and RET expression in AR positive tumors may suggest that these tumors are either a heterogeneous phenotype or are transitioning from AdCa to NEPC. Currently, little is known about the regulation of RET gene expression in prostate cancer. Several key epigenetic regulators (such as CBX2, EZH2, BRN2, and SOX2) have been identified as possible modulators that can switch tumors between an AdCa and NEPC state (5,46-48). We found that RET kinase dependency correlated with several of these transcription factors (Figure 3). Alterations in DNA methylation or transcriptional regulation resulting from the loss of proteins such as RB1 may further alter RET expression and activity. Therefore, it remains to be determined how robust RET expression is gained during the transition from mCRPC to a NEPC phenotype. In small cell lung cancer, ASCL1 was shown to induce RET gene expression and this mechanism of regulation may hold true in NEPC, but has not been validated (49).

Regardless of the dynamics of RET expression in disease progression, we showed that multiple RET kinase pathway inhibitors effectively restricted growth in the *Rb/Pten* knockout organoids and AD80 reduced the growth of the NCI-H660 cell line and spheroids *in vitro*, as well as NCI-H660 tumors *in vivo*. We validated our inhibitor studies by knocking down RET in NCI-H660 and PC3 cell lines and saw a similar reduction in overall growth. The pharmacological and genetic inhibition of RET kinase suggests that RET kinase signaling is important for NEPC tumor progression. In order to identify patients that could benefit from treatment including RET inhibition, it will be important to generate assays or validate markers of RET activity in NEPC. Pathology, loss of AR signaling, or expression of neuroendocrine genes are not sufficient alone to identify all patients with high levels of RET expression that may benefit from RET targeted therapies. Moving forward, it will be important to identify the subset of patients that would benefit from inhibition of RET kinase. Development of biomarkers for transcriptional activators,

RET protein, or markers of RET activity will enable pre-selection of individuals who would benefit from RET inhibitors. Understanding the regulation of RET gene expression, correlation of RET expression and activity and disease progression, as well as the contribution of RET kinase to mCRPC tumor progression could inform better treatment strategies.

Acknowledgements

We thank members of the Drake lab for providing advice and input on the manuscript. We also thank the members of the Biological Mass Spectrometry Facility of Robert Wood Johnson Medical School and Rutgers, The State University of New Jersey, for providing advice and performing mass spectrometry on our samples. We thank Ryder Clifford from QGel for providing reagents. We thank the patients and their families, Celestia Higano, Evan Yu, Elahe Mostaghel, Heather Cheng, Bruce Montgomery, Mike Schweizer, Andrew Hsieh, Daniel Lin, Funda Vakar-Lopez, Lawrence True and the rapid autopsy teams for their contributions to the University of Washington Medical Center Prostate Cancer Donor Rapid Autopsy Program and the Development of the LuCaP PDX models. HV is supported by Department of Defense Prostate Cancer Research Program W81XWH-19-1-0173. This work was also supported by the Department of Defense grant (W81XWH-17-1-0414; W81XWH-17-1-0415), the Prostate Cancer Biorepository Network (PCBN) (W81XWH-14-2-0183), the Pacific Northwest Prostate Cancer SPORE (P50CA97186), the PO1 NIH grant (PO1 CA163227), the Richard M. LUCAS Foundation, and the Institute for Prostate Cancer Research (IPCR). LCC and VT are supported by the National Institute of General Medical Sciences of the National Institutes of Health under award number T32 GM008339. ONW is supported by the Zimmerman Family, the Concern Foundation, and by a Prostate Cancer Foundation Challenge Award. ONW is supported by the West Coast Prostate Cancer Dream Team supported by Stand Up to Cancer/AACR/Prostate Cancer Foundation SU2C-AACR-DT0812 (ONW co-PI). This research grant is made possible by the generous support of the Movember Foundation. Stand Up To Cancer is a program of the Entertainment Industry Foundation administered by the American Association for Cancer Research. JMD is supported by the Department of Defense Prostate Cancer Research Program W81XWH-14-1-0148, W81XWH-15-1-0236 and W81XWH-18-1-0542, Prostate Cancer Foundation Young Investigator Award, and the New Jersey Health Foundation. Research reported in this publication was supported by the National Center for Advancing Translational Sciences of the National Institutes of Health Award Number UL1-TR002494, NIH Award P50 CA097186, DOD Award W81XWH-18-0347. The content is solely the responsibility of the authors and does not necessarily represent the official views of the National Institutes of Health.

References

1. Bluemn EG, Coleman IM, Lucas JM, Coleman RT, Hernandez-Lopez S, Tharakan R*, et al.* Androgen Receptor Pathway-Independent Prostate Cancer Is Sustained through FGF Signaling. Cancer Cell **2017**;32:474-89 e6
2. Beltran H, Tomlins S, Aparicio A, Arora V, Rickman D, Ayala G*, et al.* Aggressive variants of castration-resistant prostate cancer. Clin Cancer Res **2014**;20:2846-50
3. Aparicio AM, Harzstark AL, Corn PG, Wen S, Araujo JC, Tu SM*, et al.* Platinum-based chemotherapy for variant castrate-resistant prostate cancer. Clin Cancer Res **2013**;19:3621-30
4. Beltran H, Oromendia C, Danila DC, Montgomery B, Hoimes C, Szmulewitz RZ*, et al.* A Phase II Trial of the Aurora Kinase A Inhibitor Alisertib for Patients with Castration-resistant and Neuroendocrine Prostate Cancer: Efficacy and Biomarkers. Clin Cancer Res **2018**
5. Ku SY, Rosario S, Wang Y, Mu P, Seshadri M, Goodrich ZW*, et al.* Rb1 and Trp53 cooperate to suppress prostate cancer lineage plasticity, metastasis, and antiandrogen resistance. Science **2017**;355:78-83
6. Beltran H, Rickman DS, Park K, Chae SS, Sboner A, MacDonald TY*, et al.* Molecular characterization of neuroendocrine prostate cancer and identification of new drug targets. Cancer discovery **2011**;1:487-95
7. Blume-Jensen P, Hunter T. Oncogenic kinase signalling. Nature **2001**;411:355-65
8. Arighi E, Borrello MG, Sariola H. RET tyrosine kinase signaling in development and cancer. Cytokine Growth Factor Rev **2005**;16:441-67
9. Drake JM, Graham NA, Lee JK, Stoyanova T, Faltermeier CM, Sud S*, et al.* Metastatic castration-resistant prostate cancer reveals intrapatient similarity and interpatient heterogeneity of therapeutic kinase targets. Proc Natl Acad Sci U S A **2013**;110:E4762-9
10. Lee JK, Bangayan NJ, Chai T, Smith BA, Pariva TE, Yun S*, et al.* Systemic surfaceome profiling identifies target antigens for immune-based therapy in subtypes of advanced prostate cancer. Proc Natl Acad Sci U S A **2018**;115:E4473-E82
11. Ban K, Feng S, Shao L, Ittmann M. RET signaling in prostate cancer. Clin Cancer Res **2017**
12. Subbiah V, Gainor JF, Rahal R, Brubaker JD, Kim JL, Maynard M*, et al.* Precision Targeted Therapy with BLU-667 for RET-Driven Cancers. Cancer discovery **2018**;8:836-49
13. Subbiah V, Velcheti V, Tuch BB, Ebata K, Busaidy NL, Cabanillas ME*, et al.* Selective RET kinase inhibition for patients with RET-altered cancers. Ann Oncol **2018**;29:1869-76
14. Plenker D, Riedel M, Bragelmann J, Dammert MA, Chauhan R, Knowles PP*, et al.* Drugging the catalytically inactive state of RET kinase in RET-rearranged tumors. Sci Transl Med **2017**;9
15. Dar AC, Das TK, Shokat KM, Cagan RL. Chemical genetic discovery of targets and anti-targets for cancer polypharmacology. Nature **2012**;486:80-4
16. Cheng LC, Li Z, Graeber TG, Graham NA, Drake JM. Phosphopeptide Enrichment Coupled with Label-free Quantitative Mass Spectrometry to Investigate the Phosphoproteome in Prostate Cancer. J Vis Exp **2018**
17. Scheltema RA, Hauschild JP, Lange O, Hornburg D, Denisov E, Damoc E*, et al.* The Q Exactive HF, a Benchtop mass spectrometer with a pre-filter, high-performance quadrupole and an ultra-high-field Orbitrap analyzer. Mol Cell Proteomics **2014**;13:3698-708
18. Cox J, Mann M. MaxQuant enables high peptide identification rates, individualized p.p.b.-range mass accuracies and proteome-wide protein quantification. Nat Biotechnol **2008**;26:1367-72
19. Vizcaino JA, Cote RG, Csordas A, Dianes JA, Fabregat A, Foster JM*, et al.* The PRoteomics IDEntifications (PRIDE) database and associated tools: status in 2013. Nucleic Acids Res **2013**;41:D1063-9

20. Drake JM, Paull EO, Graham NA, Lee JK, Smith BA, Titz B*, et al.* Phosphoproteome Integration Reveals Patient-Specific Networks in Prostate Cancer. Cell **2016**;166:1041-54
21. Eisen MB, Spellman PT, Brown PO, Botstein D. Cluster analysis and display of genome-wide expression patterns. Proc Natl Acad Sci U S A **1998**;95:14863-8
22. Saldanha AJ. Java Treeview--extensible visualization of microarray data. Bioinformatics **2004**;20:3246-8
23. Drake JM, Graham NA, Stoyanova T, Sedghi A, Goldstein AS, Cai H*, et al.* Oncogene-specific activation of tyrosine kinase networks during prostate cancer progression. Proc Natl Acad Sci U S A **2012**;109:1643-8
24. Stoyanova T, Cooper AR, Drake JM, Liu X, Armstrong AJ, Pienta KJ*, et al.* Prostate cancer originating in basal cells progresses to adenocarcinoma propagated by luminal-like cells. Proc Natl Acad Sci U S A **2013**;110:20111-6
25. Lee JK, Phillips JW, Smith BA, Park JW, Stoyanova T, McCaffrey EF*, et al.* N-Myc Drives Neuroendocrine Prostate Cancer Initiated from Human Prostate Epithelial Cells. Cancer Cell **2016**;29:536-47
26. Park JW, Lee JK, Sheu KM, Wang L, Balanis NG, Nguyen K*, et al.* Reprogramming normal human epithelial tissues to a common, lethal neuroendocrine cancer lineage. Science **2018**;362:91-5
27. Drost J, Karthaus WR, Gao D, Driehuis E, Sawyers CL, Chen Y*, et al.* Organoid culture systems for prostate epithelial and cancer tissue. Nat Protoc **2016**;11:347-58
28. Tsherniak A, Vazquez F, Montgomery PG, Weir BA, Kryukov G, Cowley GS*, et al.* Defining a Cancer Dependency Map. Cell **2017**;170:564-76 e16
29. Cowley GS, Weir BA, Vazquez F, Tamayo P, Scott JA, Rusin S*, et al.* Parallel genome-scale loss of function screens in 216 cancer cell lines for the identification of context-specific genetic dependencies. Sci Data **2014**;1:140035
30. Schindelin J, Arganda-Carreras I, Frise E, Kaynig V, Longair M, Pietzsch T*, et al.* Fiji: an open-source platform for biological-image analysis. Nat Methods **2012**;9:676-82
31. Kumar A, Coleman I, Morrissey C, Zhang X, True LD, Gulati R*, et al.* Substantial interindividual and limited intraindividual genomic diversity among tumors from men with metastatic prostate cancer. Nat Med **2016**
32. Zhang X, Coleman IM, Brown LG, True LD, Kollath L, Lucas JM*, et al.* SRRM4 Expression and the Loss of REST Activity May Promote the Emergence of the Neuroendocrine Phenotype in Castration-Resistant Prostate Cancer. Clin Cancer Res **2015**;21:4698-708
33. Abida W, Cyrta J, Heller G, Prandi D, Armenia J, Coleman I*, et al.* Genomic correlates of clinical outcome in advanced prostate cancer. Proc Natl Acad Sci U S A **2019**;116:11428-36
34. Aggarwal R, Huang J, Alumkal JJ, Zhang L, Feng FY, Thomas GV*, et al.* Clinical and Genomic Characterization of Treatment-Emergent Small-Cell Neuroendocrine Prostate Cancer: A Multi-institutional Prospective Study. J Clin Oncol **2018**;36:2492-503
35. Beltran H, Prandi D, Mosquera JM, Benelli M, Puca L, Cyrta J*, et al.* Divergent clonal evolution of castration-resistant neuroendocrine prostate cancer. Nat Med **2016**;22:298-305
36. Mulligan LM. RET revisited: expanding the oncogenic portfolio. Nat Rev Cancer **2014**;14:173-86
37. Phay JE, Shah MH. Targeting RET receptor tyrosine kinase activation in cancer. Clin Cancer Res **2010**;16:5936-41
38. Donis-Keller H, Dou S, Chi D, Carlson KM, Toshima K, Lairmore TC*, et al.* Mutations in the RET proto-oncogene are associated with MEN 2A and FMTC. Hum Mol Genet **1993**;2:851-6
39. Dabir S, Babakoohi S, Kluge A, Morrow JJ, Kresak A, Yang M*, et al.* RET mutation and expression in small-cell lung cancer. J Thorac Oncol **2014**;9:1316-23
40. Ernani V, Kumar M, Chen AY, Owonikoko TK. Systemic treatment and management approaches for medullary thyroid cancer. Cancer Treat Rev **2016**;50:89-98

41. Gautschi O, Milia J, Filleron T, Wolf J, Carbone DP, Owen D*, et al.* Targeting RET in Patients With RET-Rearranged Lung Cancers: Results From the Global, Multicenter RET Registry. J Clin Oncol **2017**;35:1403-10
42. Smith M, De Bono J, Sternberg C, Le Moulec S, Oudard S, De Giorgi U*, et al.* Phase III Study of Cabozantinib in Previously Treated Metastatic Castration-Resistant Prostate Cancer: COMET-1. J Clin Oncol **2016**;34:3005-13
43. Sonpavde GP, Pond GR, Fizazi K, de Bono JS, Basch EM, Scher HI*, et al.* Cabozantinib for Progressive Metastatic Castration-resistant Prostate Cancer Following Docetaxel: Combined Analysis of Two Phase 3 Trials. European Urology Oncology **2018**
44. Smith DC, Smith MR, Sweeney C, Elfiky AA, Logothetis C, Corn PG*, et al.* Cabozantinib in Patients With Advanced Prostate Cancer: Results of a Phase II Randomized Discontinuation Trial. J Clin Oncol **2013**;31:412-9
45. Basch EM, Scholz M, de Bono JS, Vogelzang N, de Souza P, Marx G*, et al.* Cabozantinib Versus Mitoxantrone-prednisone in Symptomatic Metastatic Castration-resistant Prostate Cancer: A Randomized Phase 3 Trial with a Primary Pain Endpoint. LID - S0302-2838(18)30932-1 [pii] LID - 10.1016/j.eururo.2018.11.033 [doi].
46. Clermont PL, Lin D, Crea F, Wu R, Xue H, Wang Y*, et al.* Polycomb-mediated silencing in neuroendocrine prostate cancer. Clin Epigenetics **2015**;7:40
47. Bishop JL, Thaper D, Vahid S, Davies A, Ketola K, Kuruma H*, et al.* The Master Neural Transcription Factor BRN2 Is an Androgen Receptor-Suppressed Driver of Neuroendocrine Differentiation in Prostate Cancer. Cancer discovery **2017**;7:54-71
48. Mu P, Zhang Z, Benelli M, Karthaus WR, Hoover E, Chen CC*, et al.* SOX2 promotes lineage plasticity and antiandrogen resistance in TP53- and RB1-deficient prostate cancer. Science **2017**;355:84-8
49. Kosari F, Ida CM, Aubry MC, Yang L, Kovtun IV, Klein JL*, et al.* ASCL1 and RET expression defines a clinically relevant subgroup of lung adenocarcinoma characterized by neuroendocrine differentiation. Oncogene **2014**;33:3776-83

Figure Legends

Figure 1. Global phosphorylation and kinase signaling pathways are differentially regulated in AVPC cell lines compared to AdCa cell lines. A and B. Supervised hierarchical clustering heatmap of 4,235 unique phosphoserine/threonine (pS/T) enriched peptides (**Figure 1A**) and 115 unique phosphotyrosine (pY) enriched peptides (**Figure 1B**) from AdCa cell lines (Blue: C4-2, 22Rv1, LNCaP, and VCaP) and AVPC cell lines (Red: cMyc/myrAKT, LASCPC-01, EF-1, PARCB-1, PARCB-2, PARCB-3, PARCB-5, NCI-H660, DU145, and PC3). Yellow = hyperphosphorylation; Blue = hypophosphorylation. **C and D.** Kinase substrate enrichment analysis (KSEA) performed on the 10 AVPC and 4 AdCa cell lines in A and B, showed multiple predicted alterations to kinase signaling. (**Figure 1C**) KSEA for pS/T analysis used a false discovery rate (FDR) <0.05, substrate hits > 5, and normalized K score >2.0. (**Figure 1D**) KSEA for pY analysis used an FDR <0.1, substrate hits >4, and normalized K score >1.1. **E.** Phosphorylated residues identified in the global phosphoproteomics (from **Figure 1A and 1B**) or **F.** human phosphoproteome data (23) were mapped onto signaling pathways downstream of RET kinase. Yellow = Enriched in AVPC relative to AdCa; Blue = Reduced in AVPC relative to AdCa. Thick black outline = activating phosphorylation; white outline = inactivating phosphorylation; thin outline = no defined function.

Figure 2. RET kinase along with other neuroendocrine transcripts are upregulated in NEPC relative to AdCa patient samples. A. Microarray data from the University of Washington rapid autopsy data of metastatic prostate cancer biopsies (31) were clustered based on gene expression of RET, neuroendocrine markers: CHGA and ASCL1, as well as androgen regulated genes: KLK3, AR, and NKX3-1. Upregulation of expression is represented by yellow, while downregulated genes are represented by blue. Patient samples were classified by AR and NE markers as AR+NE- (green, n=134), AR-NE- (blue, n=10), AR-NE+ (red, n=20), and AR+NE+ (purple, n=7). **B.** Pearson correlation matrix of gene expression from **Figure 2A** showing a correlation of RET gene expression with neuroendocrine markers and negative correlation with AR responsive markers. **C.** Box and whisker plot of average transcript measurements of CHGA, SYP, or RET in Adenocarcinoma (AR+NE-) versus the NEPC (AR-NE+) patients. The data is represented in Tukey plots and expression values were analyzed by Student's t test. **D.** Agilent oligo array expression analysis of four neuroendocrine AR-negative LuCaP patient derived xenografts (PDX) and 20 LuCaP adenocarcinoma PDX published in *Zhang et al. 2015. Clinical Cancer Research.* (32) were clustered as in **Figure 2A**. **E.** Pearson correlation matrix of expression data represented in **Figure 2D. F.** Box and whisker plot shows an upregulation in CHGA, SYP, and RET kinase in NEPC versus AdCa PDX samples. Data is represented as in **Figure 2C**.

Figure 3. RET expression correlates with NE markers in prostate cancer cell lines and is important for NEPC cell line growth. A. RET expression dependency profiling for 11280 genes across eight prostate cell lines (PRECLH, LNCaP, VCaP, DU145, MDA PCa 2b, 22Rv1, NCI-H660, and PC3). RET expression was positively correlated with NEPC driver genes (blue) and negatively correlated with AR and AR regulators (cyan). **B.** Relative RET dependency scores reflect the ability of 503 cancer cell lines to maintain proliferation after RET knockdown (taken from the Project Achilles 2.201). Among the 8 prostate cancer cell lines, PC3 and NCI-H660 cells showed the greatest dependency on RET. **C.** RET protein expression in NCI-H660 cells stably transduced with scrambled (Scr), anti-GFP or two unique anti-RET shRNA. RET protein levels were reduced in two RET knockdown NCI-H660 cell lines and β-Actin serves as a loading control. **D.** RET knockdown reduces cellular proliferation in H660 cell lines. The line graph represents relative cellular proliferation as measured by WST assay of one biological replicate. Cell proliferation was analyzed by linear regression of log transformed data to determine statistical significance and error bars represent the standard deviation of five technical replicates.

Figure 4. NCI-H660 cells are sensitive to RET inhibition and show sensitivity to RET inhibitors. A. Immunoprecipitation of RET kinase from H660 cells shows that 4 hour treatment with 1 μM AD80, LOXO-292, or BLU-667 reduces RET tyrosine phosphorylation, as assayed with a total phosphotyrosine antibody 4G10. **B.** NCI-H660 cells treated for 4 hours with DMSO (Con) the indicated concentrations (nM) of AD80, LOXO-292, or BLU-667, showed reduced activity of the MAPK and AKT signaling cascades downstream of RET. Activity was analyzed by western blot for phosphorylation of ERK1/2 at Tyr202/Tyr204 and phosphorylation of AKT1/2 at Ser473. The AD80 treatment reduced phosphorylation of both downstream targets, while LOXO-292 and BLU-667 reduced the activity of ERK1/2. In all treatments the total ERK1/2, total AKT1/2 and Actin loading control remained unaffected. **C.** The activity of pERK1/2 (Tyr202/Tyr204) and pAKT1/2 (Ser 473) in NCI-H660 scrambled control and RET knockdown cells was assayed after a 4 hour treatment with DMSO (D), or 1μM of AD80 (A), LOXO-292 (L), or BLU-667 (B). **D.** The relative ERK1/2 activity was measured by comparing pERK1/2 (Tyr202/Tyr204) to total ERK1/2 protein and normalized to the scrambled DMSO treated sample. The ERK1/2 activity is reduced by both RET knockdown and after treatment with RET inhibitors. The bars represent the average values from three experiments and the error bars are standard deviation. **E.** Quantification of AKT1/2 activity (pAKT1/2 S473 relative to total AKT protein and normalized DMSO treated Scr cells) shows AD80 potently inhibits AKT1/2 activity while knockdown may reduce activity slightly. Bars represent the mean from three experiments and the error bars are standard deviation.

Figure 5. Organoid NEPC models are sensitive to treatment with multiple RET inhibitors. A. A dose response curve of $Pten^{-/-}$ and $Rb^{-/-}$ prostate specific double knockout (DKO) organoids treated with increasing concentrations of AD80, LOXO-292, and BLU-667. Viability was measured by staining for dead cells. Circles represent mean and error bars ± standard deviation. **B.** Bright field images and corresponding fluorescence images of GFP labeled-DKO organoids treated with the indicated concentrations of AD80. Blue=DAPI staining of nuclei, Red=Propidium iodide staining of dead cells. Scale bar =100μm. **C and D.** Representative brightfield and fluorescent images of LOXO-292 (**C**) and BLU-667 (**D**) DKO organoids treated with the indicated concentrations of drugs stained as described in E with the GFP channel omitted.

Figure 6. AD80 reduces NCI-H660 xenograft tumor growth. A. Schematic of *in vivo* study in which NCI-H660 cells were injected subcutaneously into the right flank of NOD-SCID mice and tumors were allowed to grow to approximately 100 to 200mm^3 before being randomly assigned into two treatment groups: Control (DMSO alone, n=6) or AD80 (10mg/kg/day, n=6). **B.** The fold change in tumor volume by treatment group was plotted as a function of the number of days of treatment. Means and confidence intervals (CIs) were calculated on the log scale and reported in terms of geometric means after exponentiation with error bars ± 95% confidence interval. There was evidence of an overall treatment effect on tumor growth rate (p=0.006) with a significantly lower tumor volume at day 22 (p=0.006). **C.** Average animal weights were measured at the same time as tumor volumes and no differences in average animal weight between treatment groups was observed over the duration of the study. Symbols represent means with error bars ± standard error. **D.** Following the termination of the xenograft tumor experiment, tumors were excised from animals that survived to the end of the study and photographed with a centimeter scale ruler. Separate images from the same group are divided by a white line. **E.** Representative images of H&E (2.5X and 20X), RET IHC (20X), Ki67 IHC (20X), and TUNEL (2.5X and 20X) stained sections of tumors from each group. White scale bars are 500μm. Yellow and black scale bars are 50μm. **F and G.** Average optical density of (**F**) RET staining and (**G**) Ki67 staining from five distinct fields of view in each tumor are represented by symbols with a horizontal bar representing the mean. Quantification was analyzed by one way ANOVA. **H.** Quantification of the average TUNEL positive area

679 (2.5X) was analyzed with the Kruskal-Wallis test (p=0.1727). Symbols represent averages for individual
680 tumors with a horizontal line representing the mean. Bars represent the mean with error bars represent
681 ± standard error.

Figure 1.

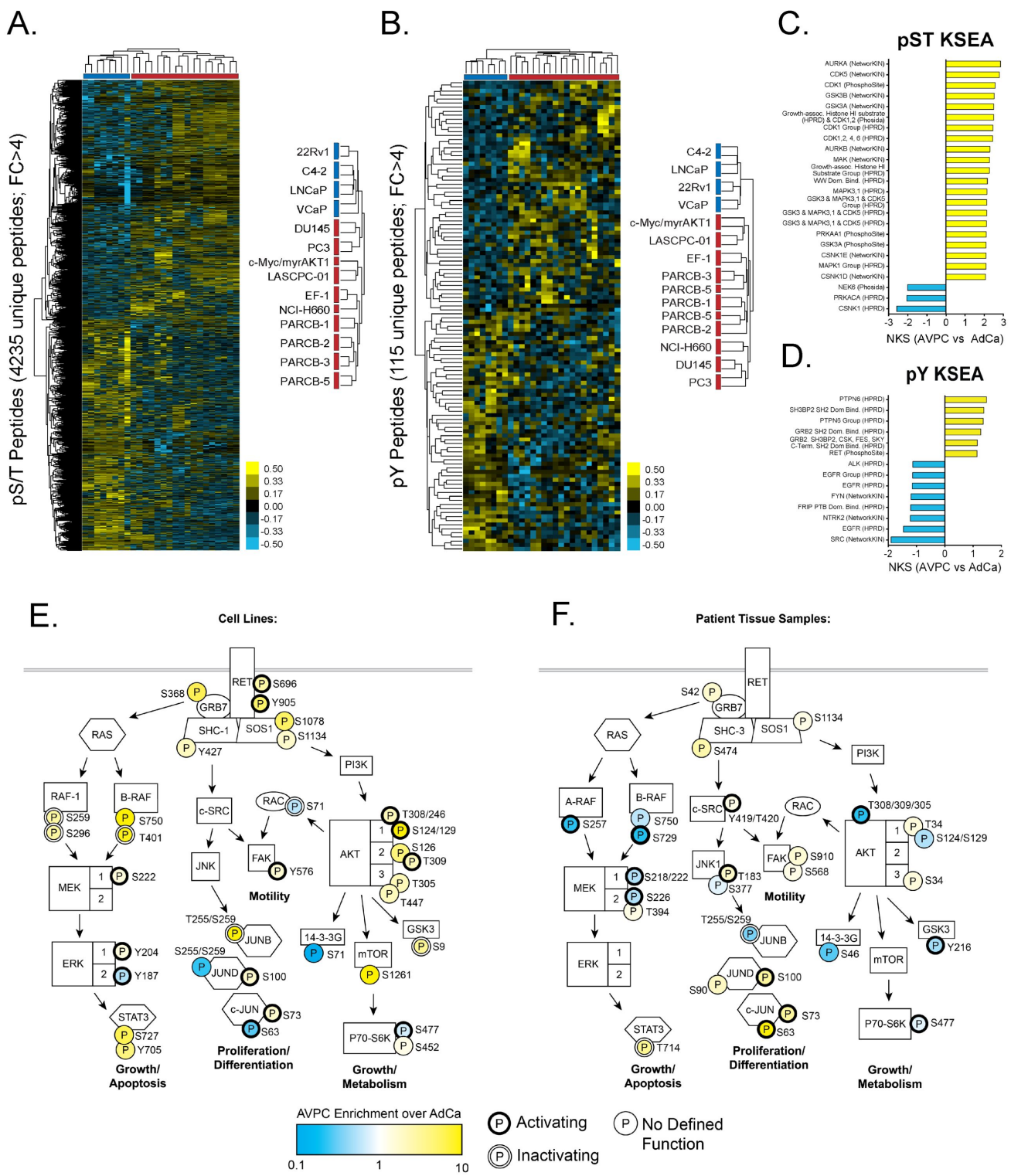
A.
pS/T Peptides (4235 unique peptides; FC>4)
22Rv1
C4-2
LNCaP
VCaP
DU145
PC3
c-Myc/myrAKT1
LASCPC-01
EF-1
NCI-H660
PARCB-1
PARCB-2
PARCB-3
PARCB-5
0.50
0.33
0.17
0.00
-0.17
-0.33
-0.50
B.
pY Peptides (115 unique peptides; FC>4)
C4-2
LNCaP
22Rv1
VCaP
c-Myc/myrAKT1
LASCPC-01
EF-1
PARCB-3
PARCB-5
PARCB-1
PARCB-5
PARCB-2
NCI-H660
DU145
PC3
0.50
0.33
0.17
0.00
-0.17
-0.33
-0.50
C.
pST KSEA
AURKA (NetworKIN)
CDK5 (NetworKIN)
CDK1 (PhosphoSite)
GSK3B (NetworKIN)
GSK3A (NetworKIN)
Growth-assoc. Histone HI substrate (HPRD) & CDK1,2 (Phosida)
CDK1 Group (HPRD)
CDK1,2, 4, 6 (HPRD)
AURKB (NetworKIN)
MAK (NetworKIN)
Growth-assoc. Histone HI Substrate Group (HPRD)
WW Dom. Bind. (HPRD)
MAPK3,1 (HPRD)
GSK3 & MAPK3,1 & CDK5 Group (HPRD)
GSK3 & MAPK3,1 & CDK5 (HPRD)
GSK3 & MAPK3,1 & CDK5 (HPRD)
PRKAA1 (PhosphoSite)
GSK3A (PhosphoSite)
CSNK1E (NetworKIN)
MAPK1 Group (HPRD)
CSNK1D (NetworKIN)
NEK6 (Phosida)
PRKACA (HPRD)
CSNK1 (HPRD)
-3 -2 -1 0 1 2 3
NKS (AVPC vs AdCa)
D.
pY KSEA
PTPN6 (HPRD)
SH3BP2 SH2 Dom Bind. (HPRD)
PTPN3 Group (HPRD)
GRB2 SH2 Dom. Bind. (HPRD)
GRB2, SH3BP2, CSK, FES, SKY
C-Term. SH2 Dom Bind. (HPRD)
RET (PhosphoSite)
ALK (HPRD)
EGFR Group (HPRD)
EGFR (HPRD)
FYN (NetworkKIN)
FRIP PTB Dom. Bind. (HPRD)
NTRK2 (NetworkKIN)
EGFR (HPRD)
SRC (NetworkKIN)
-2 -1 0 1 2
NKS (AVPC vs AdCa)
E.
Cell Lines:
RET
S368
GRB7
S696
Y905
SHC-1
SOS1
S1078
S1134
Y427
RAS
PI3K
RAF-1
S259
S296
B-RAF
S750
T401
c-SRC
RAC
S71
AKT
T308/246
S124/129
S126
T309
T305
T447
MEK
S222
JNK
FAK
Y576
Motility
T255/S259
JUNB
S255/S259
JUND
S100
14-3-3G
S71
mTOR
S1261
GSK3
S9
ERK
Y204
Y187
c-JUN
S73
S63
P70-S6K
S477
S452
STAT3
S727
Y705
Growth/
Apoptosis
Proliferation/
Differentiation
Growth/
Metabolism
F.
Patient Tissue Samples:
RET
S42
GRB7
SHC-3
SOS1
S1134
S474
RAS
PI3K
A-RAF
S257
B-RAF
S750
S729
c-SRC
Y419/T420
RAC
T308/309/305
T34
S124/S129
AKT
S34
JNK1
T183
S377
FAK
S910
S568
Motility
MEK
S218/222
S226
T394
T255/S259
JUNB
ERK
JUND
S90
S100
c-JUN
S73
S63
14-3-3G
S46
mTOR
GSK3
Y216
P70-S6K
S477
STAT3
T714
Growth/
Apoptosis
Proliferation/
Differentiation
Growth/
Metabolism
AVPC Enrichment over AdCa
0.1
1
10
Activating
Inactivating
No Defined
Function

Figure 2.

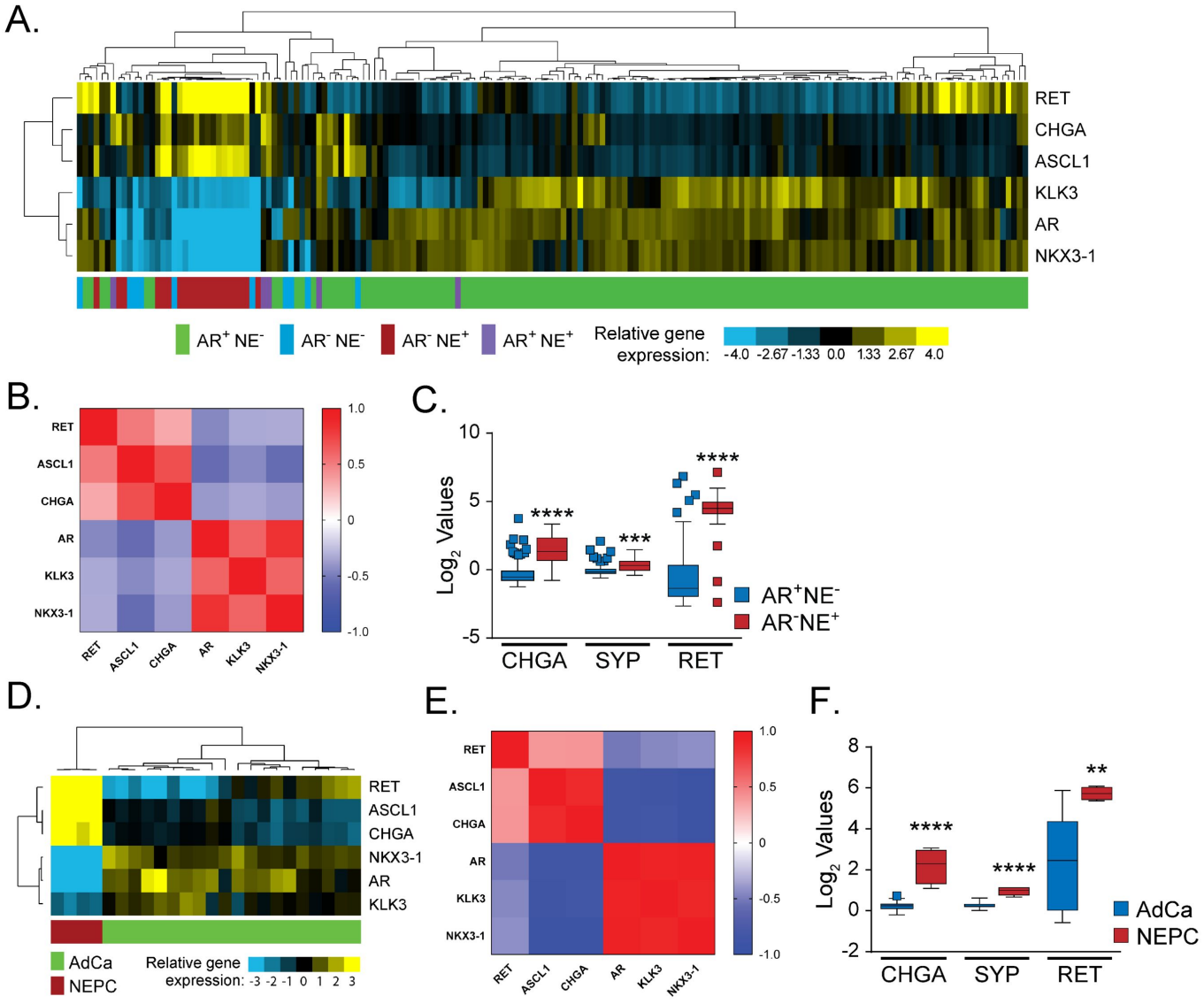
A.
RET
CHGA
ASCL1
KLK3
AR
NKX3-1
AR+ NE-
AR- NE-
AR- NE+
AR+ NE+
Relative gene expression:
-4.0 -2.67 -1.33 0.0 1.33 2.67 4.0
B.
RET
ASCL1
CHGA
AR
KLK3
NKX3-1
1.0
0.5
0
-0.5
-1.0
C.
Log2 Values
10
5
0
-5
****
***
****
CHGA
SYP
RET
AR+NE-
AR-NE+
D.
RET
ASCL1
CHGA
NKX3-1
AR
KLK3
AdCa
NEPC
Relative gene expression: -3 -2 -1 0 1 2 3
E.
RET
ASCL1
CHGA
AR
KLK3
NKX3-1
1.0
0.5
0
-0.5
-1.0
F.
Log2 Values
8
6
4
2
0
-2
****
****
**
CHGA
SYP
RET
AdCa
NEPC

Figure 3.

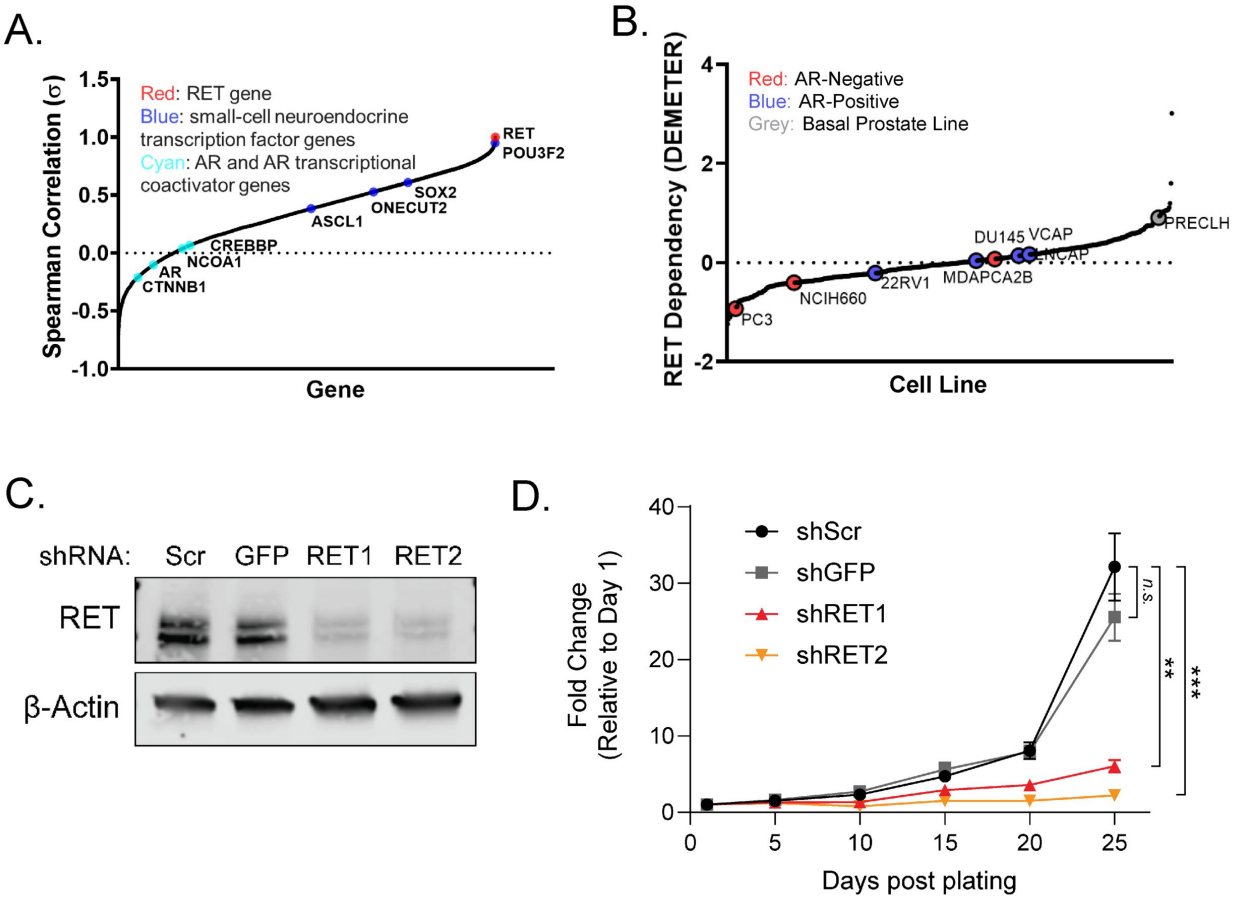
A.
Red: RET gene
Blue: small-cell neuroendocrine transcription factor genes
Cyan: AR and AR transcriptional coactivator genes
RET
POU3F2
SOX2
ONECUT2
ASCL1
CREBBP
NCOA1
AR
CTNNB1
Spearman Correlation (σ)
Gene
B.
Red: AR-Negative
Blue: AR-Positive
Grey: Basal Prostate Line
RET Dependency (DEMETER)
Cell Line
PRECLH
DU145
VCAP
LNCAP
22RV1
MDAPCA2B
NCIH660
PC3
C.
shRNA: Scr GFP RET1 RET2
RET
β-Actin
D.
shScr
shGFP
shRET1
shRET2
Fold Change (Relative to Day 1)
Days post plating
n.s.
**
***

Figure 4.

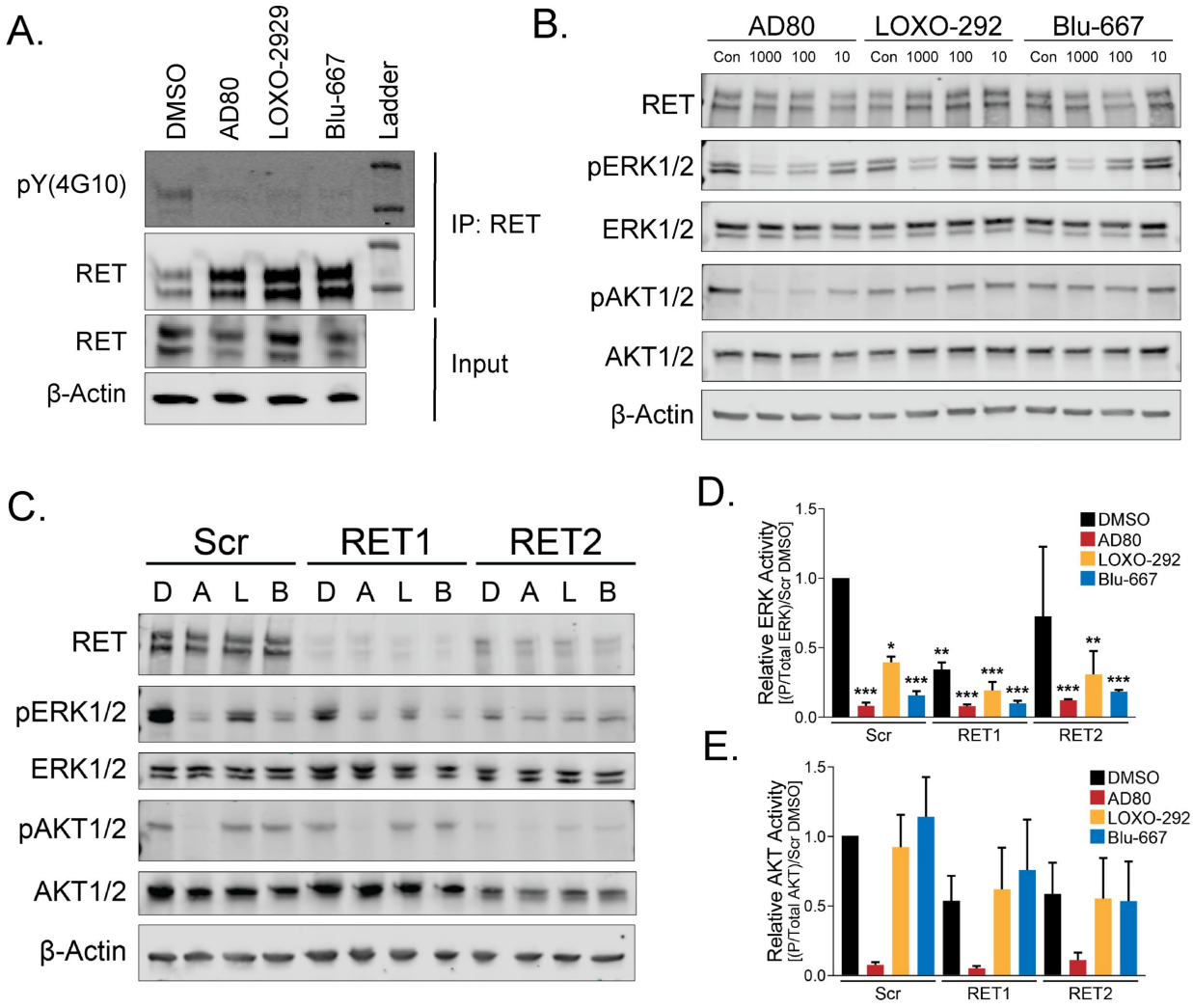
A.
DMSO
AD80
LOXO-2929
Blu-667
Ladder
pY(4G10)
RET
IP: RET
RET
β-Actin
Input
B.
AD80
LOXO-292
Blu-667
Con 1000 100 10
RET
pERK1/2
ERK1/2
pAKT1/2
AKT1/2
β-Actin
C.
Scr
RET1
RET2
D A L B D A L B D A L B
RET
pERK1/2
ERK1/2
pAKT1/2
AKT1/2
β-Actin
D.
Relative ERK Activity
[(P/Total ERK)/Scr DMSO]
DMSO
AD80
LOXO-292
Blu-667
Scr
RET1
RET2
E.
Relative AKT Activity
[(P/Total AKT)/Scr DMSO]
DMSO
AD80
LOXO-292
Blu-667
Scr
RET1
RET2

Figure 5.

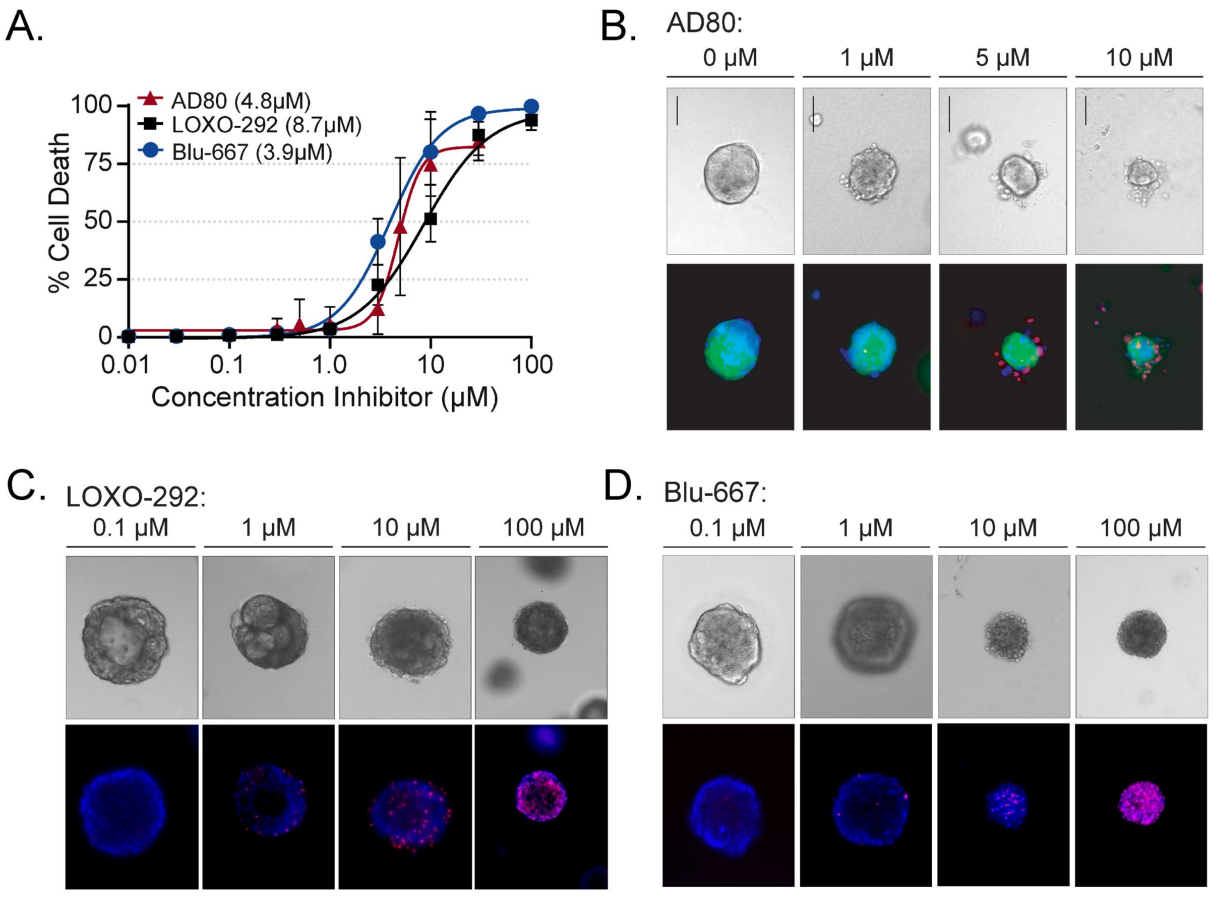
A.
AD80 (4.8μM)
LOXO-292 (8.7μM)
Blu-667 (3.9μM)
% Cell Death
100
75
50
25
0
0.01
0.1
1.0
10
100
Concentration Inhibitor (μM)
B.
AD80:
0 μM
1 μM
5 μM
10 μM
C.
LOXO-292:
0.1 μM
1 μM
10 μM
100 μM
D.
Blu-667:
0.1 μM
1 μM
10 μM
100 μM

Figure 6.

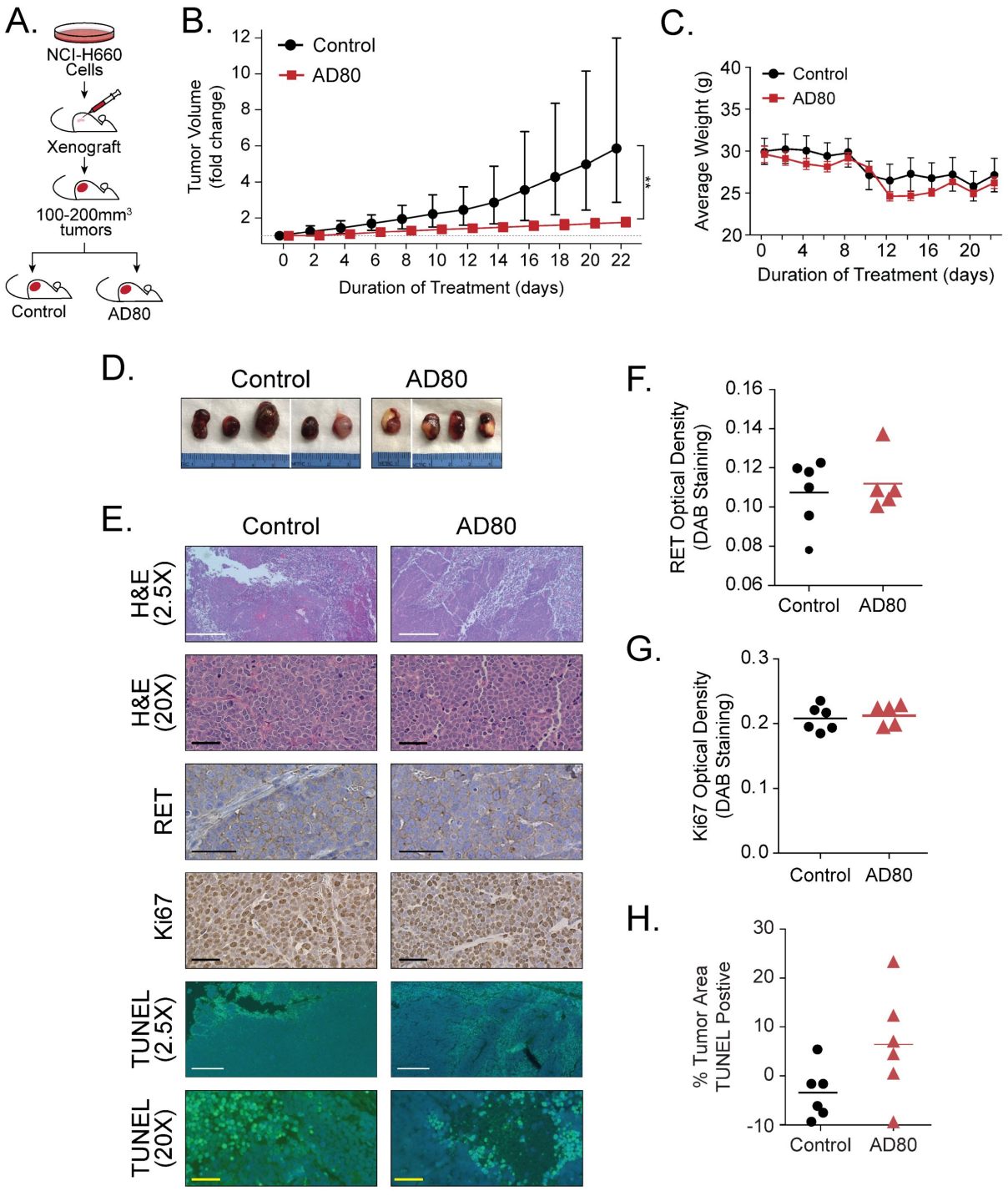
A.
NCI-H660 Cells
Xenograft
100-200mm3 tumors
Control
AD80
B.
Control
AD80
Tumor Volume (fold change)
Duration of Treatment (days)
**
C.
Control
AD80
Average Weight (g)
Duration of Treatment (days)
D.
Control
AD80
E.
Control
AD80
H&E (2.5X)
H&E (20X)
RET
Ki67
TUNEL (2.5X)
TUNEL (20X)
F.
RET Optical Density (DAB Staining)
Control
AD80
G.
Ki67 Optical Density (DAB Staining)
Control
AD80
H.
% Tumor Area TUNEL Postive
Control
AD80